Cytometry 11:586–594 (1990)

Quantitative Evaluation of Radiation-Induced Changes in Sperm Morphology and Chromatin Distribution[1]

M. Aubele,[2] U. Jütting, K. Rodenacker, P. Gais, G. Burger, and U. Hacker-Klom

Gesellschaft für Strahlen- und Umweltforschung mbH, Institut für Strahlenschutz, D-8042 Neuherberg (M.A., U.J., K.R., P.G., G.B.) and Institut für Strahlenbiologie, Universität Münster, D-4400 Münster (U.H.-K.), Federal Republic of Germany

Received for publication October 4, 1989; accepted February 13, 1990

Sperm head cytometry provides a useful assay for the detection of radiation-induced damage in mouse germ cells. Exposure of the gonads to radiation is known to lead to an increase of diploid and higher polyploid sperm and of sperm with head shape abnormalities. In the pilot studies reported here quantitative analysis of the total DNA content, the morphology, and the chromatin distribution of mouse sperm was performed. The goal was to evaluate the discriminative power of features derived by high resolution image cytometry in distinguishing sperm of control and irradiated mice. Our results suggest that besides the induction of the above mentioned variations in DNA content and shape of sperm head, changes of the nonhomogeneous chromatin distribution within the sperm may also be used to quantify the radiation effect on sperm cells. Whereas the chromatin distribution features show larger variations for sperm 21 days after exposure (dpr), the shape parameters seem to be more important to discriminate sperm 35 dpr. This may be explained by differentiation processes, which take place in different stages during mouse spermatogenesis.

Key terms: Cytometry, biological dosimetry, radiation damage,

There is a growing number of assays in male germ cell mutation research. Among these, cytometric methods offer approaches with the potential to increase speed, sensitivity, and specificity of a semen assay as well as to find new discriminative properties.

Flow cytometric measurements are frequently used to detect radiation-induced changes in DNA content in male germ cells of the mouse. By this method it could be demonstrated that cells within meiotic stages, mainly spermatocytes, are most sensitive with respect to radiation induction of diploid sperm (10,11).

Another approach to quantify radiation effects is the cytomorphometric measure of the sperm head. The relevance of sperm morphology for a genetic assay became evident 10 years ago (23,24). More recently it has been shown that the fraction of malformed sperm is related to dose and to time after exposure. Differentiated spermatogonia turned out to be the most sensitive stages for the induction of shape abnormalities (2,18). These express themselves mainly in a trend from the hook-like sperm shape toward a more circular one (25).

The goal of our study was to perform quantitative measurements, applying imaging cytometry to concentrate upon two different types of features: 1) morphological, and 2) densitometric. The rationale for the first has already been mentioned. For the second, it is the general finding that any molecular damage in sperm progenitor cells may express itself in structural changes of genome packing during sperm maturation. The latter is displayed in local redistributions of chromatin, expressed by specially derived features.

The kinetics of mouse spermatogenesis has been well described (16). Based on the developmental timetable (1), we performed our investigations on mature sperm cells in testes as well as in epididymis. In the case of the testes biopsies, these sperm had been irradiated as early spermatocytes (21 days post-radiation [dpr]), or in the case of epididymis sampling as developing sper-

[1]Supported by the Commission of the European Communities under contract no. BI6-A-172-D.

[2]Address reprint requests to M. Aubele, Gesellschaft für Strahlen- und Umweltforschung mbH, Institut für Strahlenschutz, Ingolstädter Landstraße 1, D-8042 Neuherberg, Federal Republic of Germany.

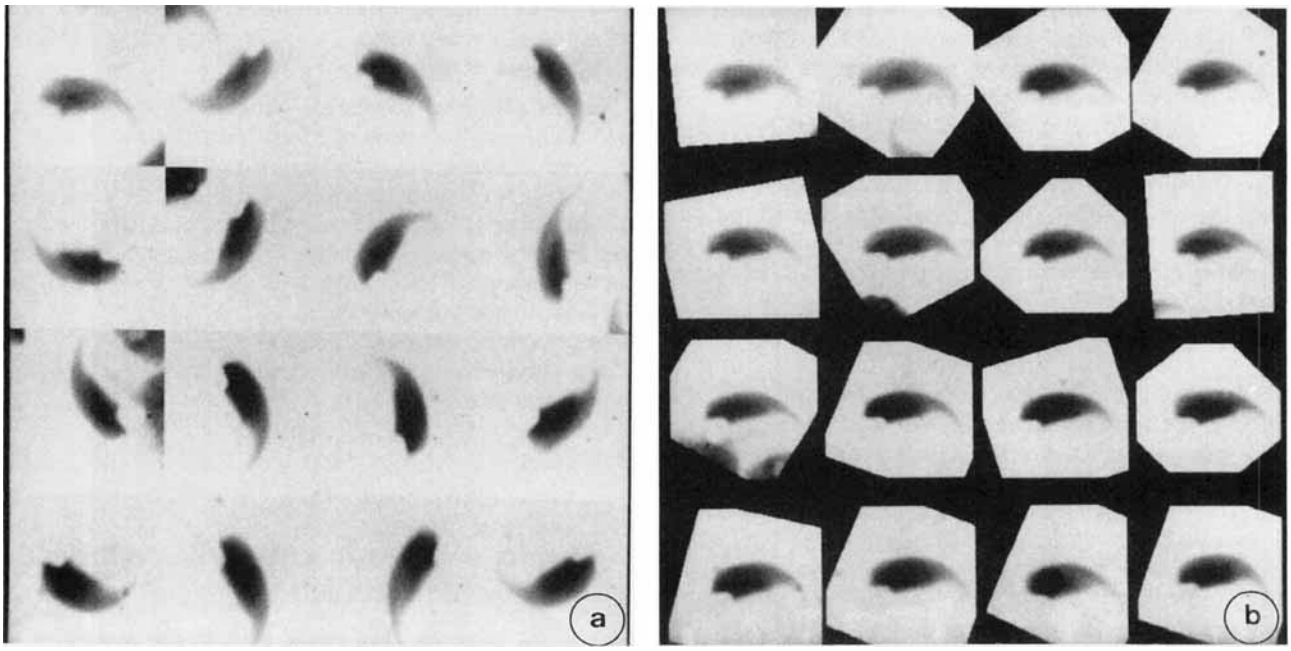

FIG. 1. **a:** Scanned images in transmission of epididymal sperm (experiment 2). **b:** The same scanning images as in a, normalized by rotation, transposition, and, if necessary, reflection, magnification, or deminuation.

matocytes (21 dpr) or as differentiated spermatogonia (35 dpr). In this way we hoped to find the most sensitive stage of spermatogenesis for the radiation induction of shape abnormalities as well as for changes in chromatin distribution.

MATERIALS AND METHODS

Preparation and Staining

Two pilot studies were performed. In the first, the material consisted of cytological specimens prepared from testicular biopsies of mice. In this case only the testes of male NMRI mice aged 8 to 10 weeks were irradiated by collimated x-rays at ten dose levels from 0.25 up to 15 Gy (200 kV, 0.5 mm Cu, 0.5 Gy/min). One set of mice received single doses, another split doses with a time lapse of 8 h in between (12). Only one mouse was available per dose. The specimens were prepared 21 days after exposure by cytocentrifugation on glass slides, fixated in methanol, and Feulgen stained (acid hydrolysis: 5N HCl, 22°C, 30 min). From each specimen up to 250 elongated spermatids were visually selected and measured by two independent observers.

In the second study, male hybrid mice (101 × C3H) aged 12 to 14 weeks were whole body irradiated with a single dose of 2 Gy Cs-137 gamma rays. They were sacrified 21 and 35 days after irradiation and mature spermatozoa were collected directly from epididymides. The sperm suspension was prepared for each mouse by mincing both epididymides into a sodium citrate solution. The cell material was then fixed in methanol and glacial acetic acid (3:1), deposited on glass slides by drops, and stained according to the Feulgen procedure already mentioned. In this experiment five animals were investigated 21 dpr and four animals 35 dpr; two were used as controls. At least one slide per mouse was prepared and 200 well-preserved spermatozoa were randomly selected and measured per slide.

Image Processing

Scanning conditions. The nuclei were scanned with an AXIOMAT-microscope (Zeiss, Oberkochen, FRG), equipped with a high resolution TV-camera (Bosch T1VK9B1, Stuttgart, FRG). The cells were measured in transmission with a 100× objective (oil immersion) and zoom factor 2.5 (Fig. 1a). The selected optical field images were digitized into 128 × 128 pixels resulting in pixel distances of 0.1 μm. The true optical resolution, assessed by measurements of the modulation transfer function (4), was about 8 times lower. Transmission was calculated pixelwise into extinction and digitized into 8 bits (256 channels). The real resolution of grey values tends to 6 bits (64 levels) (7). All measured morphometric parameters, such as perimeters or areas, are given in multiples of pixels.

Segmentation. For automated segmentation, a thresholding algorithm was applied controlled by the grey value histogram of each cell. It was followed by object selection. A slight object contour smoothing was performed by the operations of mathematical morphology "opening" and "closing" (21). Each segmented single object was inspected to avoid artefacts and to correct erroneous segmentations.

Feature extraction. The procedure for feature extraction followed standard schemes (19,20): 1) transformation of the original image, and 2) measuring inside the object in the transformed image.

Densitometric features. Densitometric features are derived from the whole object as well as from bright and dark regions, which were automatically segmented inside the object. They include features describing potential nonhomogeneous chromatin distributions inside the sperm. The transformation applied to the original image is

$$E = -150[log\ 10\ (T/240)]$$

with T being the pixel value for the transmitted light signal; E is then the extinction value of the pixel.

The measurement of a feature is performed by generation of a histogram of all object and region pixels, respectively, followed by computation of the statistical measures as sum (A), mean (M1), standard deviation (M2), kurtosis (M3), excess (M4), mode (MD), minimum (MIN), and maximum (MAX). The suffixes of feature names are given above in parentheses; the suffixes are then prefixed by an abbreviation of the object measured, e.g., for the sperm itself no prefix, for bright (Positive) and dark (Negative) regions (P) and (N), if such should occur. The list of densitometric features, e.g., results in: M1, M2, M3, for the sperm head itself; BIM1, BIM2, BIM3, for measurements inside a defined rim of the sperm head (Border Inside); PM1, PM2, PM3, for bright; and NM1, NM2, NM3, for dark particle regions inside the sperm head. The total nuclear extinction, representing DNA content per cell, is calculated by the formula: A × (M1−BGM1), where BGM1 represents the mean grey value of the Back-Ground. For deriving chromatin distribution features the flat texture (F) transformation as the difference between a median smoothed image and the original image is applied. In this transformed image dark and bright regions are segmented. Photometric features inside the segmented subareas are based on the original pixel value.

One of the most important problems in cytometric featuring is to avoid measurement uncertainties caused by preparation and staining variances. There are two methods to cope with the problem:

1. To use internal and/or external standard cells as well as highly standardized and controlled specimen preparation procedures, in order to normalize the total nuclear extinction by a factor resulting in "DNA-distributions." The factor derived for normalization may also be used to renormalize other important densitometric based features.
2. To derive and use only features which are independent of staining variability. Examples for those density features are the coefficient of variance of grey values within the sperm head (V = M2/M1) or the ratio of average grey values in certain regions, describing locally defined contrast (e.g., RPNM1 = PM1/NM1, RM1 = M1/BIM1). In addition all morphometric features, as described in the following section, are largely independent of staining.

Morphological features. Since most of the known morphological features are not invariant in terms of rotation, translation, and magnification (15), a procedure was developed to adjust and magnify the actual sperm image to a standard. This "normalized" sperm can then be compared with a reference sperm. The reported approach uses only features derived from the normalization procedure.

Geometrical normalization. For normalization purposes, the sperm is described using the following fixpoints and axes (Fig. 2a):

Fixpoints:

① top of sperm head
② centre of gravity
③ centre of the maximum inscribable circle, the centre of rotation

Axes:

-①- defined by fixpoints ① and ③
-②- through the centre of gravity ② the main axis of inertia

Rotation and transposition and, if necessary, reflection is performed in the following way:

fixpoint ③ becomes (64, 64) in image coordinates,
fixpoint ① becomes (64 + DMAX, 64) in image coordinates
with DMAX = distance between fixpoints ① and ③ (Fig. 2b)

A reflection is applied if the minimum angle between the axes -①- and -②- is negative and less than 45°. Following these operations a normalized sperm points to the left and the big arc (back) is on top (Fig. 2b). Finally, magnification or deminuation is applied. Thereby the box parameters of the actual sperm are scaled to the norm box parameters of 80, 30 (in pixels) (Fig. 2c,d). The normalized sperm heads of Fig. 1a are shown in Fig. 1b.

Morphological features. From the original sperm mask (Fig. 2a,b) the following parameters are derived:

radius of maximum inscribable circle (RMAX)
mean and standard deviation of the so-called distance function, which represents for each pixel of the sperm head the minimum distance to the border of the sperm head
distance between fixpoints ① and ③ (DMAX) and between ③ and ② (ZS)
box size (BX, BY).

Measurement and Statistical Analysis

In our first experiment, morphological measurements were not meaningful. All cell types during

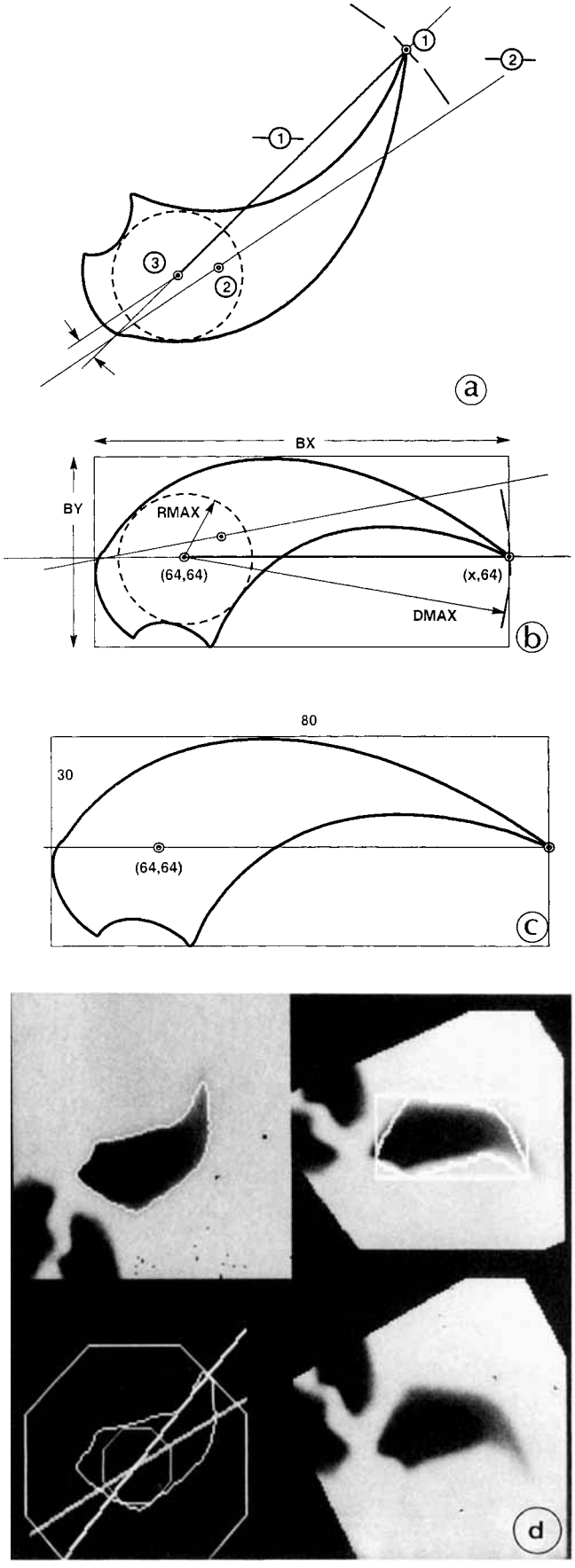

spermatogenesis are present on the slide and the shape variability of the elongated spermatids is determined to a great extent by the different degrees of maturation. Thus it is difficult to define the radiation effect morphologically. Therefore emphasis was placed upon total nuclear extinction. Nevertheless, even this measure necessitates the visual selection of mature sperm. As radiation, especially at higher doses, may lead to cell degeneration, the definition of elongated spermatids is not trivial. We have therefore performed two studies with independent investigators. One has trained himself to select only typical nondegenerated sperm with clear heads, more or less pronounced tips at the apical or tail regions, and rather homogeneously distributed chromatin (UJ); the other accepted every clearly elongated spermatid including all degrees of degeneration (MA). Each measured between 100 and 300 cells per specimen.

The total nuclear extinction (TNE) of each cell was calculated. The frequency distributions of the TNE of all measured cells per specimen were normalized to the same average of the haploid 1c-line. The relative amount of spermatids and spermatozoa in a specimen with a DNA content above a threshold set at 1.5 c was plotted as a function of dose.

In the second experiment, the cells were pooled into three classes: controls, 2 Gy at 21 days after irradiation (dpr), and 2 Gy at 35 dpr. It is the rationale of the second experiment, that radiation effects less severe than block of meiosis can be measured. Such more marginal effects may be expressed in a continuous manner by a greater population of cells depending on the real microdosimetric event and hence primary damage distribution within cells. Therefore single cell classifications were performed by means of a stepwise linear discriminant analysis (LDA) (3) using either morphometric features only or densitometric and morphometric ones. In these classification tasks, many features are generally offered and stepwise selected on the basis of F-statistics. In Table 3 the F-value for the first feature is the univariate value, for the following the additional impact. The maximal number of features used in any single classification task was restricted to eight. The description for cited features is given in Table 1.

RESULTS

First Experiment

Fig. 3 shows as example the DNA-distributions measured by the first investigator for the single dose ex-

FIG. 2. Sperm head in an arbitrary position and size with: **a:** The description of the fixpoints and the derived features. (1), top of sperm head; (2), centre of gravity; (3), centre of rotation; -(1)-, axis defined by the fixpoints (1) and (3); -(2)-, main rotational axis. **b:** Rotation, transposition, and, if necessary, reflection of the sperm head. **c:** Magnification or deminuation for the normalization of the sperm size. **d:** Geometrical normalization of a measured sperm by the above mentioned steps.

Table 1
Description of the Features Used in the Different Classifications

A	Area of sperm in pixels
P	Perimeter
NM1	Mean extinction value of the dark particles
BIM1	Mean of the grey value distribution of the rim
BIM2	Standard deviation of the grey value distribution of the rim
RDM1	Difference of mean grey value of the sperm and of the rim
RM1	Ratio of mean grey value of the total sperm head (M1) and of its rim (BIM1)
FPAA	Ratio of the area of the bright particles and the total area
FNAA	Ratio of the area of the dark particles and the total area
DISTM2	Standard deviation of the distance function
ZS	Euclidean distance between the centre of rotation and the centre of gravity
DMAX	Maximal diameter
P × P/A	Form factor
BX/BY	Ratio between box sizes after normalization

periment. Fig. 4 shows the dose effect curves (fraction of sperm with DNA > 1.5 c) of both investigators for the single dose and for the split dose experiment. The mean value of the fraction [probability (*P*)] of nonhaploid sperm and its 95% confidence interval based upon binomial statistics is plotted. The following trends are obvious: If only nondegenerated spermatids are measured, both the single and split dose curves are nonlinear (Fig. 4a). If all elongated spermatids are accepted the single dose curve becomes more linear, but not the split dose curve (Fig. 4b). In both cases the split dose effects are lower than the single dose effects.

Second Experiment

In our second experiment with 2 Gy whole body irradiation, the relative amount of spermatozoa with a DNA content > 1.5 c was 0.3% in the pooled controls, 4.4% in the pooled sperm 21dpr, and 3.3% in the spermatozoa 35 dpr. This agrees well with the data of experiment I.

The main data analysis for the second experiment is done by LDA. In a first step only morphometric features were applied to investigate the role of shape variations, and in a second step densitometric features were also added after normalization of the DNA distributions. Using only morphometric features in the three class case (control–21dpr–35dpr) results in a total correct cell classification rate of 56%. The most important feature was the perimeter of the sperm. When applying all features the correct cell classification rate was increased to 75.8% (Table 2) and the feature chosen with the highest discrimination power was RM1, the ratio of the mean grey values of the whole object and the rim

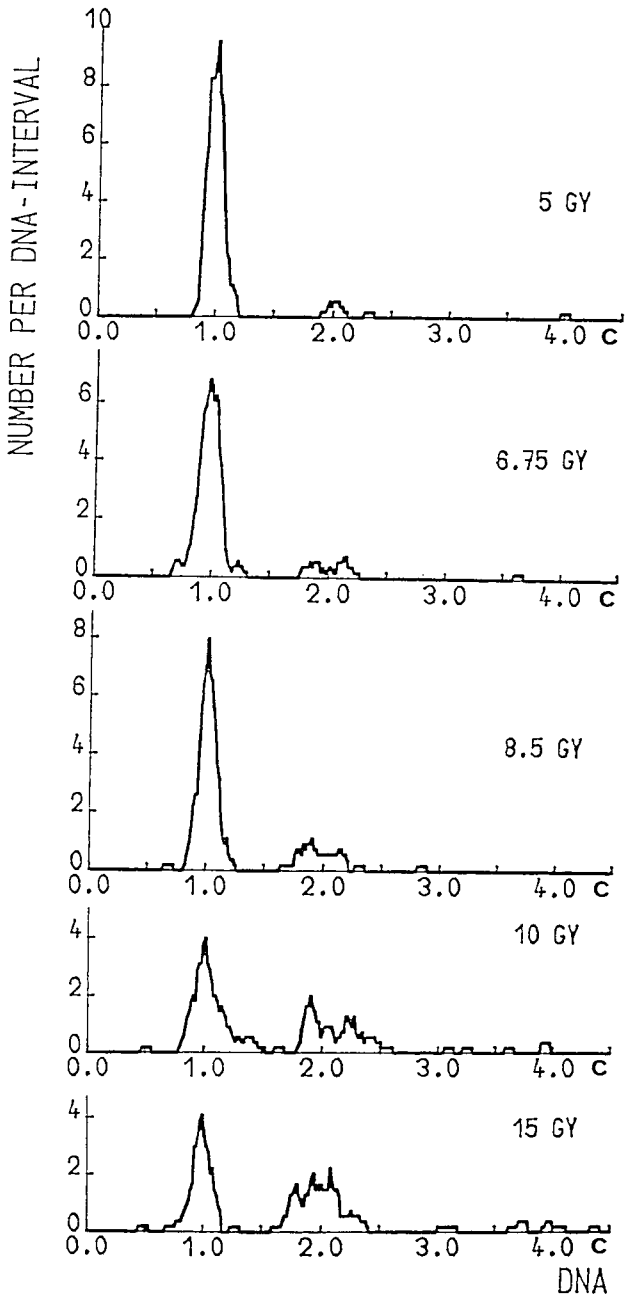

FIG. 3. DNA distributions for the single dose experiment for five different doses (first experiment), measured by investigator UJ. Each distribution represents an arithmetically smoothed histogram based on about 200 measured elongated spermatids.

(Table 3). In Table 4 the mean values and the standard deviations of the most important features are given. Fig. 5 shows the distribution of the three pooled cell classes in the two-dimensional feature space of the first two canonical variables. The mean values of the three populations are marked. From this the general trend of the sperm of irradiated mice as a function of time after exposure is clearly demonstrated. There is also no ev-

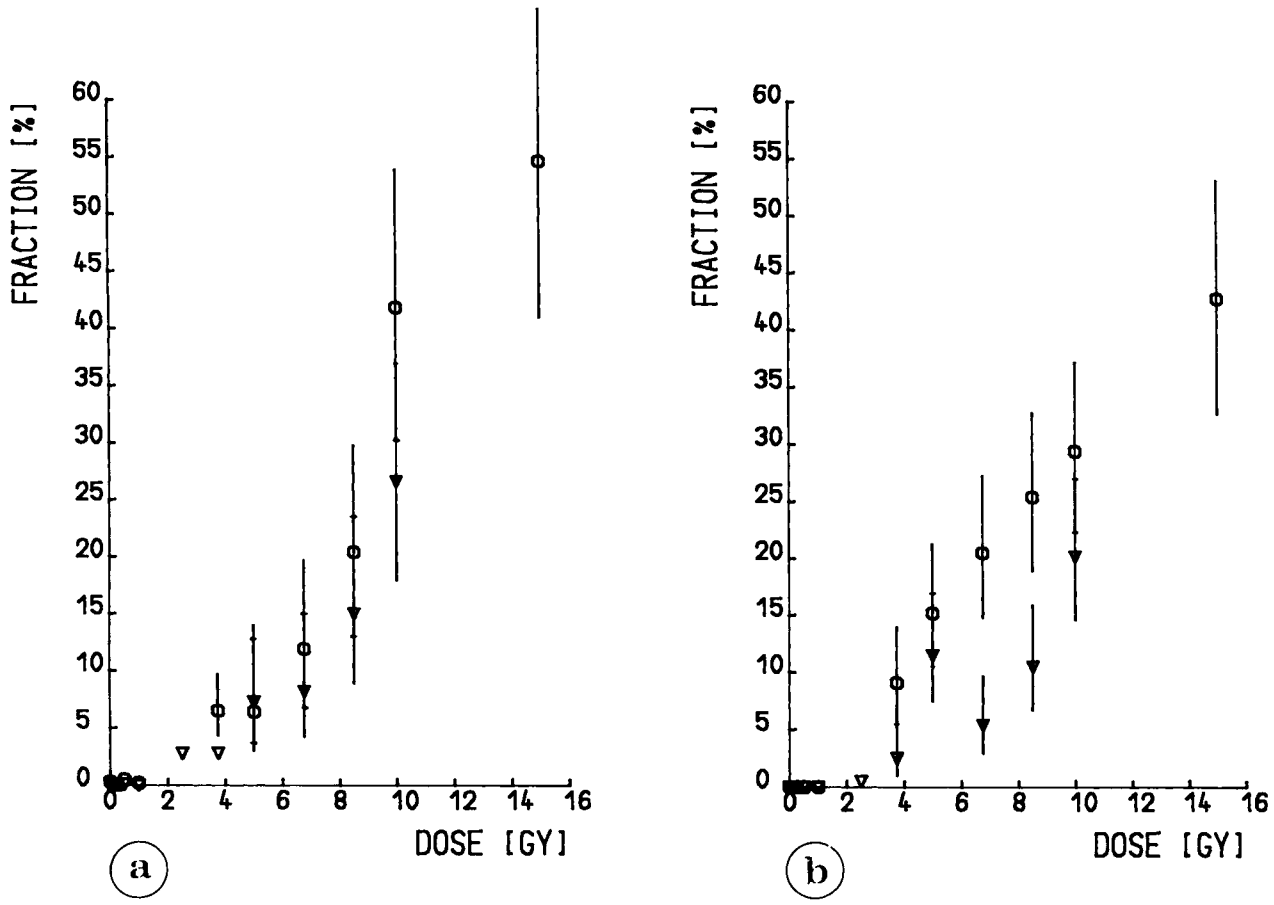

FIG. 4. The dose effect curves of both investigators for the fraction of cells with DNA content > 1.5 c (first experiment). ○, single dose; ▽, split dose. **a:** Dose curves measured by observer UJ, accepting only nondegenerated elongated spermatids. **b:** Dose curves measured by observer MA, accepting all degrees of degeneration. The error bars shown give the mean value of the probability (P) of non-haploid sperm and its 95% confidence interval.

Table 2
Cell Classification Matrix for the Three Groups (See Also Table 3) Morphometric and Densitometric Features ($P < 0.0001$)

	Control	dpr 21	dpr 35	% Correct
Control	623	141	39	77.6
21	72	967	169	80.1
35	95	164	543	67.7
Total				75.8

Table 3
The Most Important Features and Their F-Values (Multivariate) for the Discrimination of the Three Classes When Offering of Morphometric and Densitometric Features

Selected feature	F-value
RM1 = M1/BIM1	421.0
P	257.3
NM1	184.8
BIM2	251.0
RDM1	122.4
FPAA	256.1
P × P/A	73.0

idence that this trend may be artificially initiated by statistical outliers due to the low number of cases available.

The cell classification rate for the binary case (control–21 dpr) was 88.3%. The best feature for this discrimination was again RM1, followed by other densitometric features. The best feature for the classification case (control–35-dpr) was DMAX, a shape feature. The cell classification rate for this case was 88.9%. If one plots RM1 versus DMAX for all sperm it becomes more evident that the main cytometric changes at 21 dpr concern the chromatin, but at 35 dpr essentially the sperm shape. This is shown schematically in Fig. 6. To prove the obvious trends of the pooled populations, we calculated also the Mahalanobis distances from each 21-dpr- and 35-dpr-specimen to the controls. There was no evidence that these trends are caused by specimen outliers. The last three features of Table 4, DMAX, P ×

Table 4
Mean Values and SD of the Most Important Features for Discrimination of Three or Two Cell Groups

	Control		21 dpr		35 dpr	
Feature	Mean	SD	Mean	SD	Mean	SD
RM1	1.3	0.09	1.2	0.06	1.3	0.1
NM1	18.7	2.6	22.3	5.1	21.8	4.3
BIM2	4.5	0.9	4.9	1.7	4.5	1.5
FPAA	0.11	0.03	0.13	0.03	0.12	0.02
P	197.0	12.2	187.9	14.3	182.2	14.8
P × P/A	22.4	1.6	22.4	2.2	20.9	2.1
BX/BY	2.4	0.2	2.3	0.3	2.2	0.3
DMAX	49.4	4.5	45.6	5.5	43.7	5.7

P/A, and the ratio of the box parameters BX/BY, are derived shape factors which demonstrate that with increasing time after exposure with 2 Gy the sperm heads seem to become more circular shaped.

DISCUSSION

The radiobiological model behind our findings in the first experiment may be as follows. Elongated spermatids, measured 21 days after exposure in testes biopsies, were diploid secondary and some even tetraploid primary spermatocytes when irradiated. Radiation damage may lead to the following endpoints:

1. Complete meiosis and rather complete maturation with some morphological changes of the haploid spermatids
2. Block of meiosis, leading to diploid and (less frequently) even hyperdiploid spermatids with rather complete maturation and some morphological changes
3. Degenerative changes in both haploid and multiploid elongated spermatids with incomplete maturation

For possible interpretation of the dose effect curves shown in Fig. 4 let us first concentrate on the single dose experiments. Observer UJ, who selected only nondegenerated elongated spermatids, clearly gets a nonlinear dose effect curve which at the highest dose level already seems to bend off indicating the theoretically expected sigmoidal shape (Fig. 4a). Observer MA, on the other hand, accepted all degrees of degeneration and gets a more linear dose effect curve (Fig. 4b).

This finding may be explained as follows: Only the mature cells, either haploid or diploid, are released into the epididymes and disappear from the observable cell pool. The more or less degenerated ones, which have undergone different degrees of maturation and/or retardation, remain in the testis. So it is conceivable that the relative amount of degenerated diploid spermatids is higher than that of mature ones for relatively low doses. At high doses more and more exposed haploid sperm may just get to the maturation step of elongation but then degenerate. As a consequence the dose effect curves expressing cellular fractions will bend off. The low dose region cannot be assessed for statistical reasons.

Summing up, there may be cell populations expressing different degrees of maturation with different kinetics occuring in the testes after the block of meiosis. Depending on selection criteria the dose effect curves found are sigmoidal or linear. These findings explain the linear dose relationship published earlier for the same experiment, with the fraction of nonhaploid cells detected by flow cytometry (12). However, the results do not support the hypothesis that radiation damage to sperm progenitor cells should generally result in linear dose effect relationships. The split dose experiments, despite the large uncertainty in the measurements, clearly show nonlinear behaviour for both observers.

In our second experiment both feature sets, densitometric and shape, seem to be useful for biological monitoring of sperm of the mouse. The classification results show different sensitivities of the two feature sets applied: the sperm from irradiated mice 21 dpr differ mostly from the control cells by densitometric features, displaying the local distribution of chromatin in the sperm head; the irradiated sperm 35 dpr differ by shape features (Fig. 6). These results agree with earlier findings that differentiated spermatogonia (35 dpr) are more sensitive with respect to the radiation-induction of malformed sperm (17,18,25). The different sensitivities of our two feature sets may be explained by the various differentiation processes during mouse spermatogenesis (9).

During the transformation of spermatids into mature sperm, the chromatin undergoes a dramatic exchange of histones for sperm-specific basic proteins, which allows a more compact packaging of the chromatin (5,9,14). The chromatin condensation starts in the elongated spermatids at the top of the sperm head and progress towards the posterior region (6,9). This process may be responsible for our findings of chromatin changes expressed more at 21 dpr than at 35 dpr. It is likely that irradiation during this process affects the condensation and thus causes a different chromatin distribution in the mature sperm, measurable by densitometric features.

The formation of the normal sperm head involves a series of morphological and biochemical steps (2). The reason for abnormal head shapes is not yet clear. Nevertheless it can be assumed that many genes are involved in the morphology of the normal sperm (23) and it is supposed that these genes are expressed at the diploid level, before meiotic segregation of chromosomes (8,13,22). These genes may be affected by irradiation, and greater degrees of malformed sperm may be observed at 35 dpr than at 21 dpr.

It can be concluded that the measurement of DNA abnormalities and morphology of sperm may represent a rapid and simple assay for radiation-induced damage on spermatogonial cells in vivo. Additionally we demonstrate that densitometric features provide a powerful method to study the radiation response in sperm.

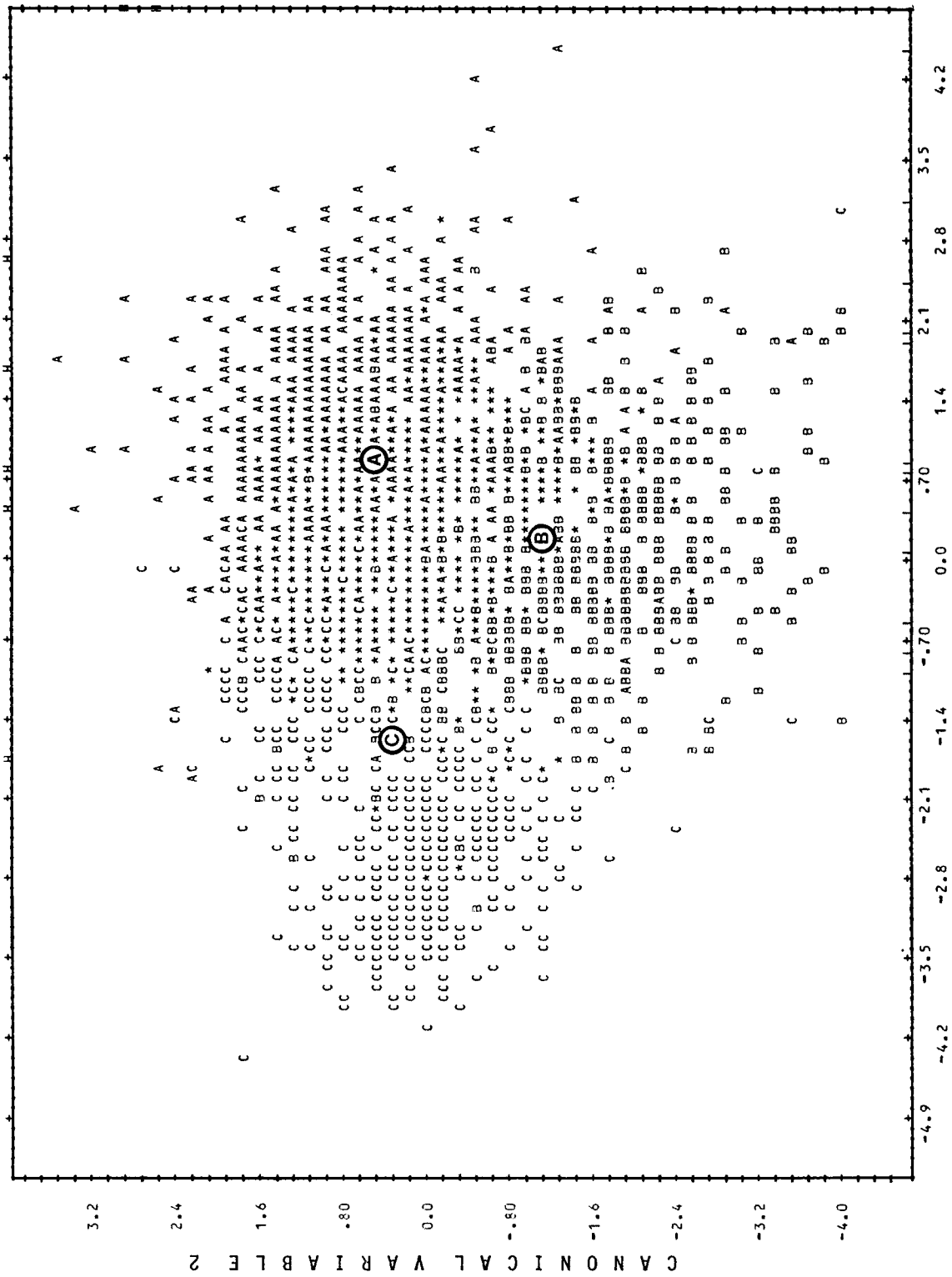

FIG. 5. Distribution of the three pooled cell classes (second experiment) in the two-dimensional feature space of the first two canonical variables. A, sperm 21 dpr (Ⓐ = mean value); B, sperm 35 dpr (Ⓑ = mean value); C, control cells (Ⓒ = mean value). Different cells with identical values are indicated by asterisks.

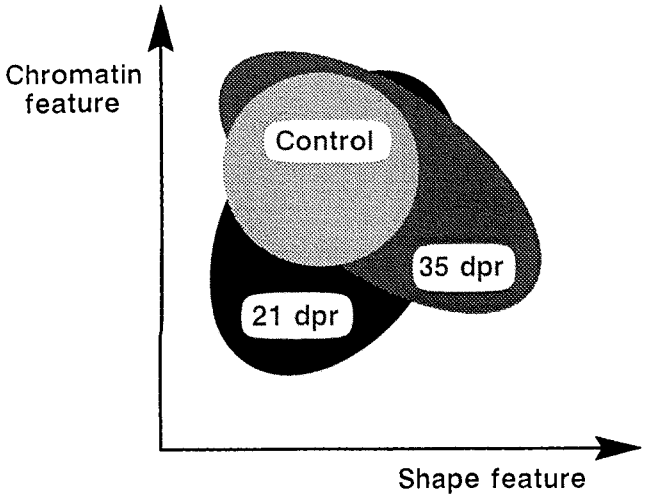

FIG. 6. Scheme of the three sperm populations (second experiment): trends of the different populations for the best densitometric (RM1) and shape (DMAX) feature.

ACKNOWLEDGMENTS

The authors would like to thank Dr. I.-D. Adler and her group from the Department of Genetics Gesellschaft für Straulen-und Umweltforschung mnbH (GSF) for kindly supplying laboratory facilities and the mice used in our second experiment.

LITERATURE CITED

1. Adler ID: Male germ cell cytogenetics. In: Cytogenetic Assay of Environmental Mutagens, Hsu TC (ed). Allanheld, Osmun, NJ, 1982, pp 249–276.
2. Bruce WR, Furrer R, Wyrobek AJ: Abnormalities in the shape of murine sperm after acute testicular x-irradiation. Mut Res 23: 381–386, 1974.
3. Burger G, Jütting U: Specimen classification in cytometry: an intercomparison of various means of decision making. In: Pattern Recognition in Practise II, Gelsema ES, Kanal LN (eds). North Holland Public., Amsterdam, 1985, p 509–519.
4. Burger G, Jütting V, Gais P, Rodenacker K, Schenck U: Anwendung der hochauflösenden Bildanalyse in der medizinischen Zytometrie. In: Morphometrie in der Zyto- und Histopathologie, Burger G, Oberholzer M, Gössner W (Hgb). Springer Verlag, 1988, pp 200–226.
5. Evenson DP, Darzynkiewicz Z, Melamed MR: Comparison of human and mouse sperm chromatin structure by flow cytometry. Chromosoma 78:225–238, 1980.
6. Evenson DP, Higgins PJ, Melamed MR: Detection of male reproductive abnormalities by flow cytometry measurements of testicular and ejaculated germ cells. In: Biological Dosimetry, Eisert WG, Mendelsohn ML (eds). Springer Verlag, 1984, pp 99–109.
7. Gais P, Burger G: Geräte zur quantitativen Mikroskopie. In: Morphometrie in der Zyto- und Histopathologie, Burger G, Oberholzer M, Gössner W (Hgb). Springer Verlag, 1988, pp 282–294.
8. Gledhill BL: Studies of the DNA content dry mass and optical area of morphologically normal and abnormal bull spermatozoal heads. Acta Vet Scand 7:1–20, 1966.
9. Guraya SS: Biology of Spermatogenesis and Spermatozoa in Mammals. Springer Verlag, 1987, pp 110–124.
10. Hacker-Klom U, Göhde W, Schumann L: Mammalian spermatogenesis as a biological dosimeter for ionizing radiation. In: Biological Dosimetry, Eisert WG, Mendelsohn ML (eds). Springer Verlag, 1984, pp 127–137.
11. Hacker-Klom U, Göhde W, Schumann J: Quantitative evaluation of spontaneous and radiation-induced polyploidisation processes in human and murine testes. Acta Radiol Oncol 24:6:503–507, 1985.
12. Hacker-Klom U, Heiden Th, Otto FJ, Mauro F, Göhde W: Radiation-induced diploid spermatids in mice. Int J Radiat Biol 55: 797–806, 1989.
13. Martin RH, Rademaker A: The relationship between sperm chromosomal abnormalities and sperm morphology in humans. Mut Res 207:159–164, 1988.
14. Mayer JR, Zirkin BR: Spermatogenesis in the mouse: I. Autoradiographic studies of nuclear incorporation and loss of 3H amino acids. J Cell Biol 81:403–419, 1979.
15. Niemann H: Klassifikation von Mustern. Springer Verlag, Berlin, 1983.
16. Oakberg EF: A new concept of spermatogonial stem cell renewal in the mouse and its relationship to genetic effects. Mutat Res 11:1–7, 1971.
17. Oakberg EF: Response of spermatogonia of the mouse to hycanthone: a comparison with the effect of gamma rays. In: Physiology and Genetics of Reproduction, Part A, Coutinho EM, Fuchs F (eds). Plenum Publishing, New York, 1974.
18. Pinkel D: Cytometric analysis of mammalian sperm for induced morphologic and DNA content errors. In: Biological Dosimetry, Eisert WG, Mendelsohn ML (eds). Springer Verlag, 1984, pp 111–126.
19. Pratt EK: Digital Image Processing. John Wiley & Sons, New York, 1978, p 532.
20. Rodenacker K: Featuring of cellular objects. In: Clinical Cytometry and Histometry, Burger G, Ploem JS, Goerttler K (eds). Academic Press, London, 1987, pp 91–96.
21. Serra J: Image analysis and mathematical morphology. Academic Press, London, 1982.
22. Wyrobek AJ, Heddle JA, Bruce WR: Chromosomal abnormalities and the morphology of mouse sperm heads. Can J Genet Cytol 17:675–681, 1975.
23. Wyrobek AJ, Bruce WR: The induction of sperm-shape abnormalities in mice and humans. In: Chemical Mutagens, Vol.5,11, Hollaender A, de Serres FJ (eds). Plenum Publish. Corporation., 1978, pp 257–285.
24. Wyrobek AJ: Changes in mammalian sperm morphology after x-ray and chemical exposures. Genetics 92:s105–s119, 1979.
25. Young IT, Gledhill BL, Lake S, Wyrobek AJ: Quantitative analysis of radiation-induced changes in sperm morphology. Anal Quant Cytol 4:207–214, 1982.